Aptamer-Conjugated DNA Icosahedral Nanoparticles As a Carrier of Doxorubicin for Cancer Therapy

Microsugar Chang,[†,‡] Chung-Shi Yang,[†] and Dong-Ming Huang[†,*]

[†]Center for Nanomedicine Research, National Health Research Institutes, Miaoli, Taiwan, and [‡]Institute of Molecular Medicine, National Tsing-Hua University, Hsinchu, Taiwan

ABSTRACT DNA can be used to nanofabricate three-dimensional (3D) polyhedra. A variety of applications of 3D DNA assemblies have been proposed. Drug encasulation and intracellular delivery using DNA nanoparticles, however, have remained a challenge. Here, we create a distinct five-point-star motif and aptamer-conjugated six-point-star motif using well-used primer sequences to intermolecularly construct DNA icosahedra as a nanocarrier for doxorubicin. Aptamer-conjugated doxorubicin-intercalated DNA icosahedra (Doxo@Apt-DNA-icosa) show an efficient and specific internalization for killing epithelial cancer cells.

KEYWORDS: DNA nanoparticle · aptamer · controlled drug release · targeted delivery · cancer therapy

In the past decade, a series of reports have shown that DNA can be used to fabricate not only two-dimensional (2D) nanopatterns[1−4] but also three-dimensional (3D) polyhedra.[5−11] RNA, sharing great similarity with DNA, despite being more labile than DNA, has also advanced significantly in nanotechnology.[12−14] A variety of applications of 3D DNA assemblies have been proposed; according to the tensegrity principle that triangular faces will lead to rigid structures,[15−17] DNA icosahedra would be expected to be rigid and resistant to deformation and hence could potentially serve as nanocages.[11] Recently Mao *et al*. made a breakthrough in DNA nanofabrication by designing a five-point-star motif to assemble DNA icosahedra;[15] however, the intangible DNA architecture remains a major challenge.[17] In addition, to our knowledge, no report has shown that 3D DNA assemblies are likely capable of intracellular delivery, since oligonucleotides cannot traverse cell membranes. However, short, single-stranded oligonucleotides known as aptamers[18,19] have been shown to be able to recognize cellular surface receptors and thus have been used to import the wanted nanoparticles, but not 3D DNA nanoparticles, into targeted cells. Two general approaches could be imagined to modify 3D DNA nanoparticles' surface with aptamers. One is postmodification after the construction of DNA assemblies; however, the modification methods have not yet been developed. The other is premodification before the assembling onset of 3D DNA nanostructure, in which aptamer sequences should be the end-segments of DNA strands and could be allowed to be located on the outside of DNA nanoparticles. However, with the use of a premodification method in such as Mao's strategy, we suggest that those DNA polyhedra might fail to form or that aptamers might fail to adopt a distinct 3D conformation due to the interference of a complicated intra- or intermolecular interaction of the polyhdera with aptamers. Doxorubicin, a widely used drug in cancer chemotherapy,[20−22] is an anthracycline antibiotic. Closely related to the natural product daunomycin, and like all anthracyclines, it works by intercalating DNA,[23,24] a feature that also render its intercalation capability in DNA nanoparticles. Here, without the aid of a computer program to design DNA sequences, we create a distinct five-point-star motif (and six-point-star motif) using well-used primer sequences to intermolecularly construct DNA icosahedra as a nanocarrier for doxorubicin. DNA aptamers were conjugated to doxorubicin-intercalated DNA icosahedra to efficiently and specifically kill epithelial cancer cells.

RESULTS AND DISSCUSSION

Our approach to forming DNA icosahedra is illustrated in Figure 1A: In a one-pot process, five individual DNA single strands (I, II, III, IV, and V) are first assembled into sticky-ended five-point-star motifs and then further assembled into icosahedra through sticky-end association between the tiles. Each single strand, which contains 48 nucleotides, can be subdivided into three

* Address correspondence to dmhuang@nhri.org.tw.

Received for review February 20, 2011 and accepted July 5, 2011.

Published online July 06, 2011
10.1021/nn200693a

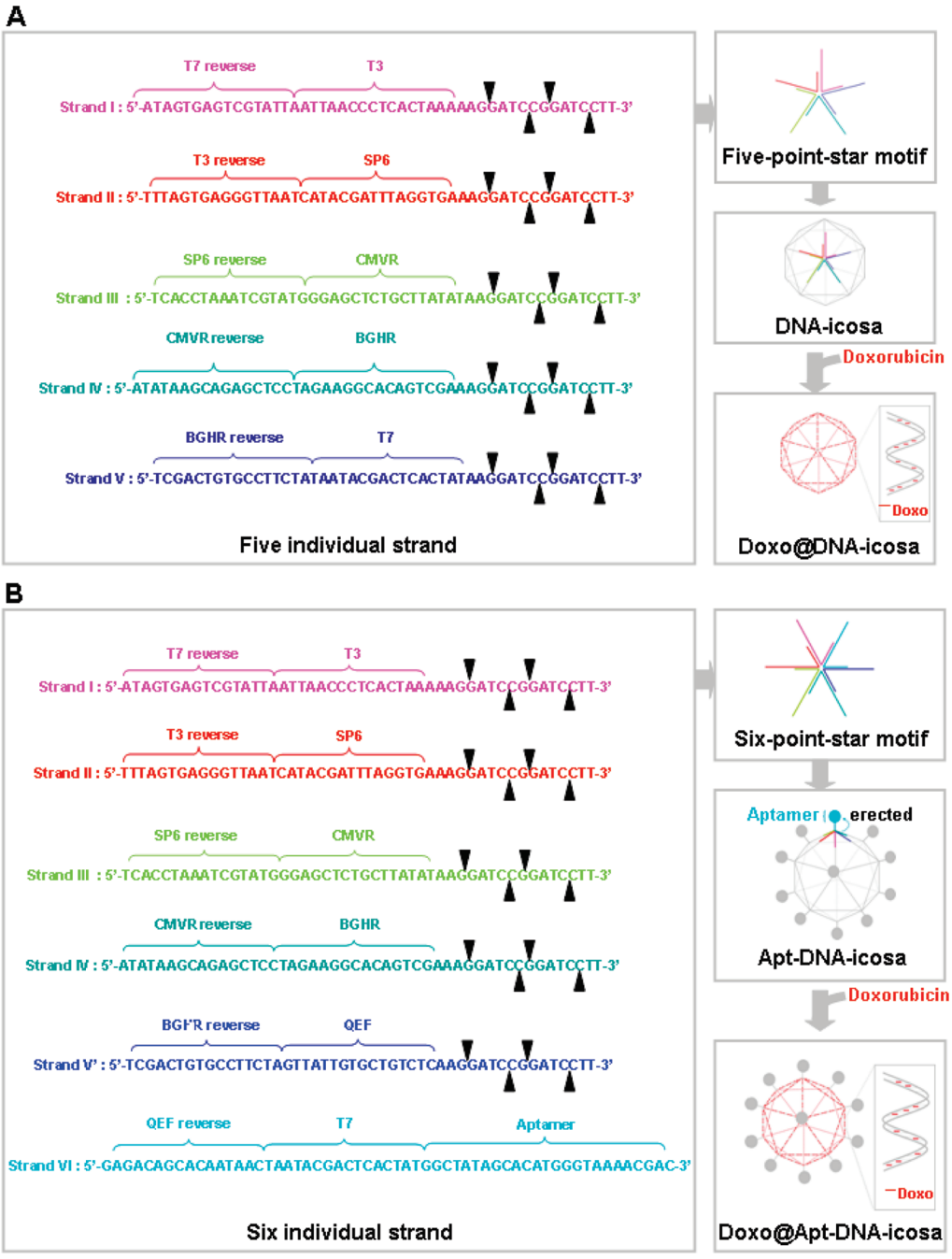

Figure 1. Scheme of self-assembly of DNA icosahedra. (A) Five DNA strands stepwise assemble into sticky-ended five-point-star motifs. Five-point-star motifs then further assemble into DNA-icosa. (B) Six DNA strands assemble into sticky-ended six-point-star motifs. Six-point-star motifs then further assemble into Apt-DNA-icosa. Doxorubicin is then intercalated into both DNA-icosa and Apt-DNA-icosa. The doxorubicin-intercalated area is highlighted.

16-nucleotide segments. The first two segments of each strand are complementary to those of the other two neighboring strands and point to the center of the five-point-star motif. The sequences of the first two segments were derived from primer sequences that have been widely used in autosequencing for decades. These widely used primer sequences could guarantee the successful forming of icosahedra because nonspecific binding and internal stem loop formation could be reduced. The third segment as the sticky end possesses a palindrome sequence that contains double restriction endonuclease *Bam*HI sites for its characterization. The palindrome sequence was also designed in order to make individual tiles' sticky ends complementary with each other.

Six individual DNA single strands for forming aptamer-conjugated DNA-icosahedra (shown as Apt-DNA-icosa) are shown in Figure 1B. MUC 1 is an important class of tumor surface marker that is uniquely and abundantly expressed on a broad range of epithelial

cancer cells.[25,26] These markers are also rapidly recycled through intracellular compartments[27,28] and thus can serve as entry portals for aptamers.[29] Therefore, the MUC 1 aptamer sequence identified in a previous study[29] was used as the end segment of strand VI. Also in a one-pot process, six individual DNA single strands (I, II, III, IV, V′, and VI) were first assembled into sticky-ended six-point-star motifs, with five of these strands (I, II, III, IV, and V′) bending to a specific angle to hybridize with adjacent tiles, and strand VI standing alone. Bending of the five strands erected aptamer-containing strand VI; eventually, all the tiles assembled into icosahedra through sticky-end association. Doxorubicin was then incorporated into DNA-icosa (Doxo@DNA-icosa) and Apt-DNA-icosa (Doxo@Apt-DNA-icosa), where dsDNA serves as the docking site for doxorubicin (Figure 1).

The assembly of DNA icosahedra was characterized by multiple techniques, including agarose gel electrophoresis (AGE), dynamic light scattering (DLS), and transmission electron microscopy (TEM). In AGE, a clear band (both DNA-icosa and Apt-DNA-icosa) with high molecular weight is observed on the gel when correct molecular concentrations of DNA strands (1000 nM for each strand) are used, suggesting that the assembly of the large DNA complex is concentration dependent (noted as a red star at the lower-right corner of the band; Figure 2A). The yields of DNA-icosa and Apt-DNA-icosa assembly are ~79% and ~75%, respectively, as estimated by AGE (1000 nM for each DNA strand in Figure 2A). It is notable that a weak band with low molecular weight appears in a negative correlation with the concentrations of DNA strands (noted as a yellow star at the lower-right corner of the band; Figure 2A). The low molecular band corresponds to the expected size of either the five-point-star motif (120 bp) or aptamer-conjugated six-point-star motif (144 bp). DLS studies reveal that after cooling for 48 h the large DNA complex was formed by incubating these 5 or 6 DNA strands (1000 nM for each strand) and possesses an apparent hydrodynamic diameter of 28.2 ± 3.0 nm for DNA-icosa and 28.6 ± 5.0 nm for Apt-DNA-icosa (Figure 2B). These values are very close to that of the diameter of the designed DNA icosahedron. To provide direct evidence for the assembly of DNA into DNA-icosa and Apt-DNA-icosa, we have imaged the DNA samples by TEM (Figure 2C). Figure 2C shows all the DNA complexes as well-structured, icosahedrally shaped particles either before or after doxorubicin intercalation. These results suggest that the five-point-star and six-point-star tiles have been assembled into the DNA-icosa and Apt-DNA-icosa, respectively.

The identification and doxorubicin intercalation efficiency of Doxo@DNA-icosa and Doxo@Apt-DNA-icosa are shown in Figure 2D. Various concentrations (from 1 to 1000 μM) of doxorubicin were mixed with DNA-icosa (800 nM) and Apt-DNA-icosa (800 nM). These DNA samples then underwent incubation at room temperature for 1 h, followed by centrifugation. Dark red precipitates were found at the bottom of every individual tube, indicating doxorubicin-intercalated DNA icosahedra. The doxorubicin intercalation efficiency of Doxo@DNA-icosa gradually increases with increasing concentration of doxorubicin, while that of Doxo@Apt-DNA-icosa remains steady. About 40% of doxorubicin was intercalated into both Doxo@DNA-icosa and Doxo@Apt-DNA-icosa when 1000 μM doxorubicin was used. Accordingly, about 1200 molecules of doxorubicin were associated with a particle. This intercalation condition was used in the following experiments. The data suggest a simple and efficient doxorubicin intercalation into DNA icosahedra.

Next, a MUC1-negative cell line, a Chinese hamster ovary cell line (CHO-K1; MUC1$^-$), and a MUC1-postive human breast cancer cell line (MCF-7; MUC 1$^+$) were used to examine the capacity and specificity of cellular internalization and the cytotoxicity of Doxo@Apt-DNA-icosa. Flow cytometry showed a higher cellular internalization efficiency of Doxo@Apt-DNA-icosa than Doxo@DNA-icosa in MCF-7 cells but not in CHO-K1 cells, suggesting an aptamer-mediated internalization of DNA nanoparticles and a cell selectivity of this internalization (Figure 3A). Moreover, the cellular internalization of Doxo@Apt-DNA-icosa in MCF-7 cells was concentration-dependent (Figure 3A). Confocal microscopy also showed that only Doxo@Apt-DNA-icosa efficiently internalized into MCF-7 cells and that the distribution of doxorubicin surrounded the nucleus (Figure 3B).

In order to further confirm the aptamer-mediated cellular selectivity of internalization of Doxo@Apt-DNA-icosa, CHO-K1 cells were prelabeled with green dye (Vybrant DiO cell-labeling solution) and then co-cultured with MCF-7 cells for Doxo@Apt-DNA-icosa internalization determination. The co-cultures were treated with free doxorubicin, Doxo@DNA-icosa, and Doxo@Apt-DNA-icosa and then examined using confocal microscopy. In all treated groups, CHO-K1 cells were observed in green fluorescence; however, MCF-7 cells could be detected only with red fluorescence of doxorubicin in the Doxo@Apt-DNA-icosa-treated group (Figure 3C). Moreover, there was no observation of the co-localization between Vybrant green and doxorubicin red (Figure 3C). To prove the specific interaction between Doxo@Apt-DNA-icosa and MUC 1, a cold competition assay for cellular internalization study was performed. Flow cytometry shows that MUC 1-specific aptamers could prohibit the cellular internalization of Doxo@Apt-DNA-icosa in MCF-7 cells (Figure 3D), indicating the specific interaction between Doxo@Apt-DNA-icosa and MUC 1. The data demonstrate that MUC 1 aptamers efficiently and specifically deliver Doxo@Apt-DNA-icosa into MUC 1$^+$ MCF-7 cells.

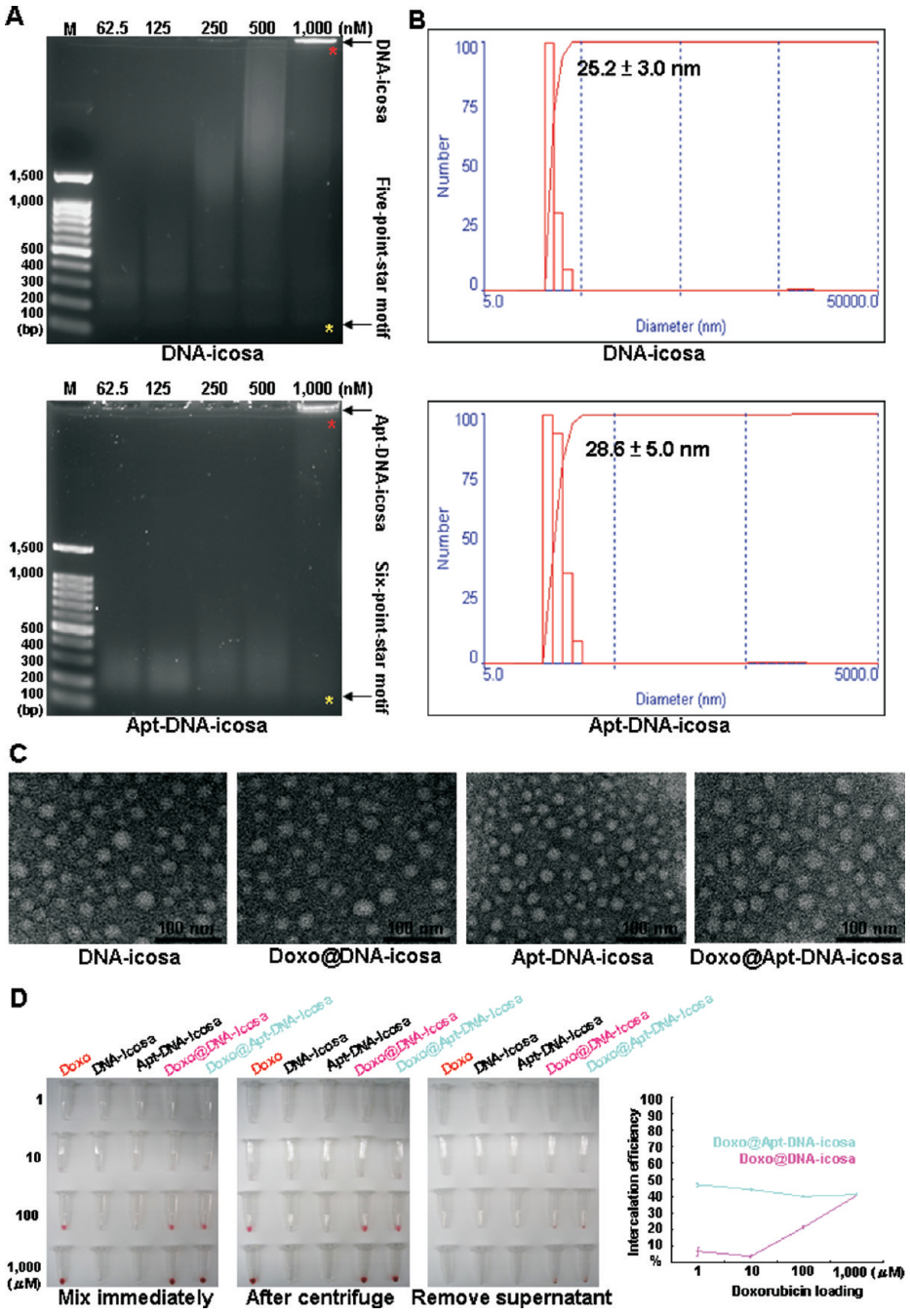

Figure 2. Characterization and doxorubicin intercalation of DNA icosa and Apt-DNA-icosa. (A) Agarose gel electrophoresis (2%) analysis of the self-assembly DNA-icosa and Apt-DNA-icosa. Various concentrations (from 62.5 to 1000 nM) of individual DNA strands (equal molecular ratio for each strand) were tested to find the optimal concentration for forming DNA-icosa and Apt-DNA-icosa. Lane M: 100 bp DNA ladder marker. (B) DLS analysis shows the size of DNA-icosa and Apt-DNA-icosa. (C) TEM images shows the structure of DNA-icosa and Apt-DNA-icosa (stained with EtBr and then negative stained with AM and trehalose) and Doxo@DNA-icosa and Doxo@Apt-DNa-icosa (only negative stained with AM and trehalose). (D) Various concentrations (from 1 to 1000 nM) of doxorubicin were mixed with DNA-icosa and Apt-DNA-icosa to determine their intercalation efficiency. Lane 1 is doxorubicin (1 to 1000 nM). Lanes 2 and 3 are DNA-icosa and Apt-DNA-icosa, respectively. Lanes 4 and 5 are doxorubicin mixed with DNA-icosa and Apt-DNA-icosa, respectively. Samples were imaged immediately after they were mixed; after centrifugation they were incubated for 1 h at room temperature; then their supernatant was removed. The pellets for Doxo@DNA-icosa and Doxo@Apt-DNA-icosa were analyzed to determine doxorubicin intercalation efficiency. About 50 nmol of doxorubicin was intercalated into 200 pmol of DNA (DNA-icosa and Apt-DNA-icosa) when 1000 μM doxorubicin was used.

In the cytotoxicity study using MTT assay, no significant difference of cell viability was observed among free doxorubicin-, Doxo@DNA-icosa-, and Doxo@Apt-DNA-icosa-treated CHO-K1 cells; however, in MCF-7 cells, Doxo@Apt-DNA-icosa indeed showed a greater cytotoxicity than free doxorubicin

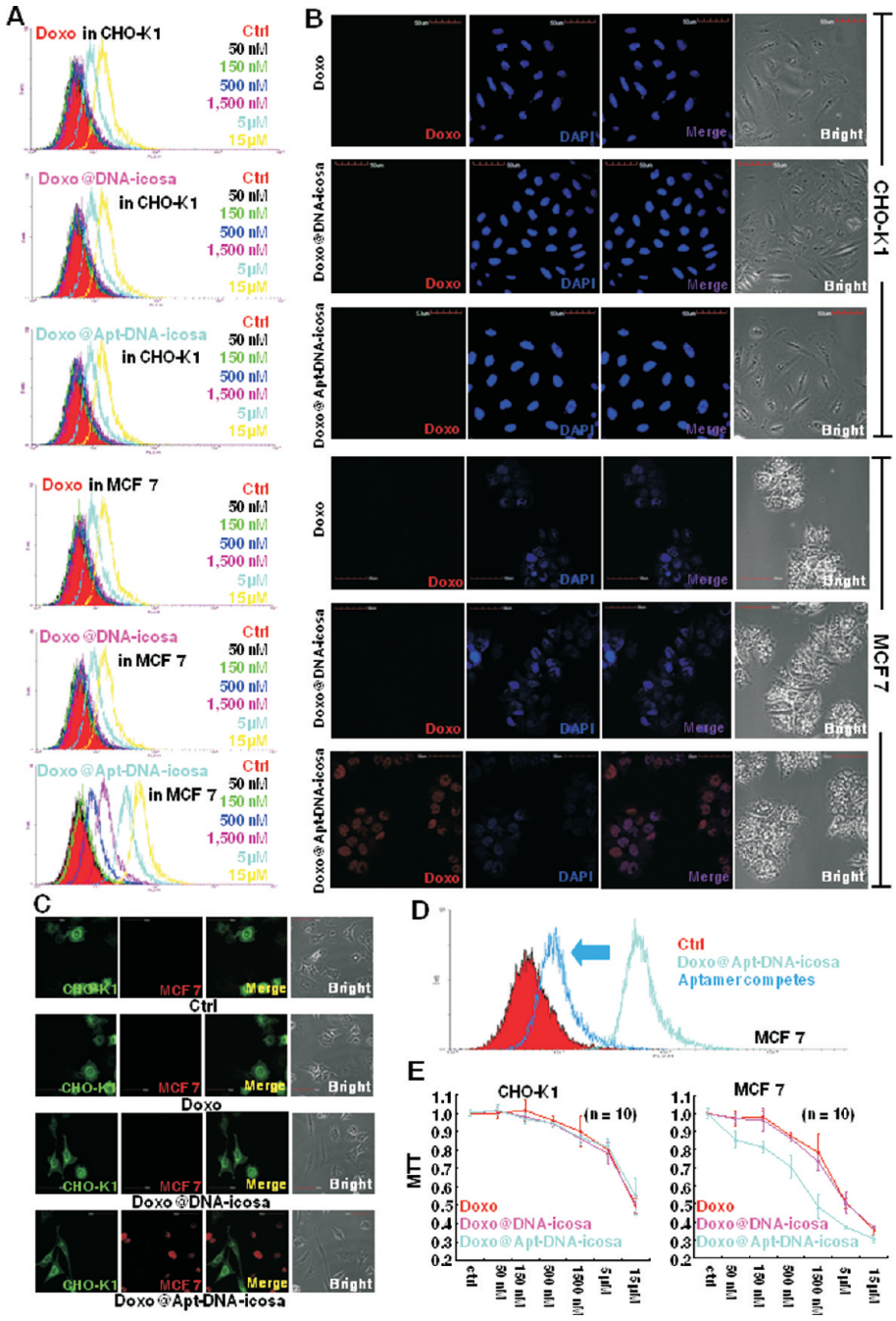

Figure 3. Selective binding and delivery of Doxo@Apt-DNA-icosa to MUC 1$^+$ cells. (A) CHO-K1 (MUC 1$^-$) and MCF-7 (MUC 1$^+$) cells were treated with vehicles (PBS; Ctrl), doxorubicin (Doxo), Doxo@DNA-icosa, or Doxo@Apt-DNA-icosa with the indicated concentration. Flow cytometry shows the binding efficiency and dosage-dependent manner of Doxo@Apt-DNA-icosa compared with doxorubicin and Doxo@DNA-icosa. (B) Cells were treated with 15 μM doxorubicin (Doxo), Doxo@DNA-icosa, or Doxo@Apt-DNA-icosa. Confocal images show that Doxo@Apt-DNA-icosa but not doxorubicin or Doxo@DNA-icosa specifically internalized into MCF-7 cells. Nucleus was stained with DAPI. (C) CHO-K1 cells prelabeled with Vybrant dye and co-cultured with MCF-7 cells. Co-cultures were treated with vehicle (PBS; Ctrl), 15 μM doxorubicin (Doxo), Doxo@DNA-icosa, or Doxo@Apt-DNA-icosa. Confocal images demonstrate the selectivity and internalization of Doxo@Apt-DNA-icosa compared with doxorubicin and Doxo@DNA-icosa. (D) MCF-7 cells were treated with vehicle (PBS; Ctrl), Doxo@Apt-DNA-icosa (doxorubicin, 15 μM), or Doxo@Apt-DNA-icosa plus free aptamer (400 nM) for competition assay and analyzed by flow cytometry. (E) CHO-K1 and MCF-7 cells were treated with doxorubicin (Doxo), Doxo@DNA-icosa, or Doxo@Apt-DNA-icosa at the indicated concentrations. MTT assay shows the cytotoxicity of Doxo@Apt-DNA-icosa compared with Doxo and Doxo@DNA-icosa.

and Doxo@DNA-icosa (Figure 3E). These results not only indicate a specific and efficient delivery of anticancer drug-intercalated DNA nanoparticles but also suggest a potential for targeted cancer therapy.

MUC1 is internalized by dynamin-dependent and clathrin-mediated endocytosis and turns over by degradation in lysosomes.[28] To examine whether the internalization of Apt-DNA-icosa was mediated by

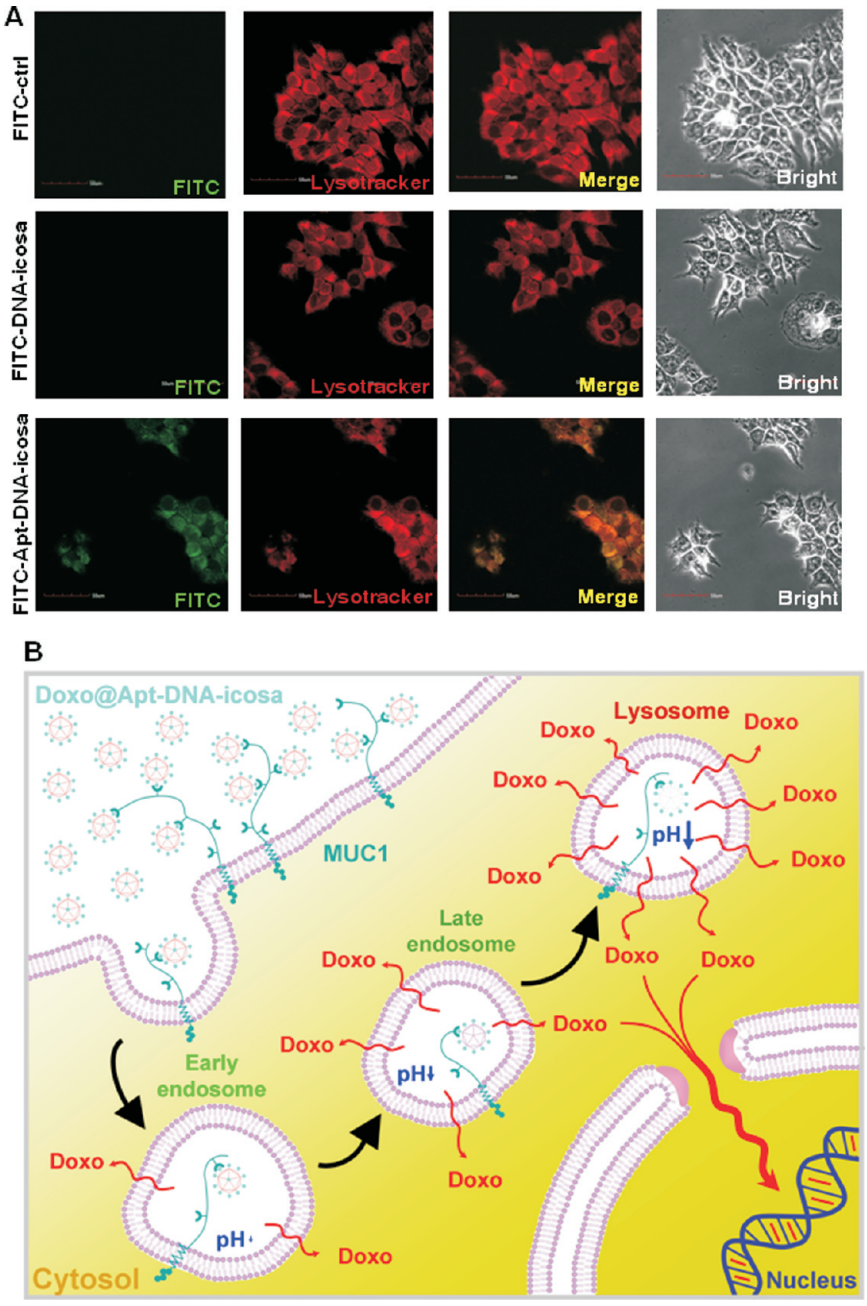

Figure 4. Intracellular distribution of Apt-DNA-icosa and its cytotoxic mechanism in MCF-7 cells. (A) MCF-7 cells were treated with FITC (40 nM), FITC-DNA-icosa, and FITC-Apt-DNA-icosa. Lysosomes were stained with LysoTracker Red (Molecular Probes). Confocal images show the co-localization of FITC-Apt-DNA-icosa and lysosomes. (B) Proposed mechanism of action of Doxo@Apt-DNA-icosa. Doxo@Apt-DNA-icosa initially recognizes MUC 1, which is then recycled through intracellular compartments. Doxo@Apt-DNA-icosa is smuggled to intracellular compartments by binding to MUC 1. Doxorubicin is gradually released through the entire recycling pathway and significantly released (Figure S1) when Doxo@Apt-DNA-icosa migrates to acid compartments, such as lysosomes. Doxorubicin in turn migrates to the nucleus and intercalates chromosome DNA, thus inducing cell death.

endocytosis, FITC-modified Apt-DNA-icosa was used and its intracellular distribution was analyzed by confocal microscopy. Confocal images show the fluorescence signal of FITC partially overlapped with LysoTracker Red (Figure 4A), suggesting an endocytosis of Apt-DNA-icosa and a localization of Apt-DNA-icosa in lysosomes. The mechanism of cellular internalization of Doxo@Apt-DNA-icosa is illustrated in Figure 4B.

CONCLUSIONS

In conclusion, we have shown that DNA icosahedra can be assembled in a simple and rapid way from five DNA strands based on a five-point-star motif. Extending from the novel idea, six DNA strands, one of which with a specific aptamer sequence built-in, can first form a six-point-star motif in 2D and then be constructed into 3D DNA icosahedra with the

exposure of aptamers to their outside. This method might serve to produce nanocarriers not only to store/intercalate and specifically deliver the anticancer drug doxorubicin into targeted cells for cancer therapy but also to perform controlled release by environmental pH (Figure S1).

MATERIALS AND METHODS

Oligonucleotides. DNA sequences are as follows. Strand I: 5′-ATAGTGAGTCGTATTAATTAACCCTCACTAAAAAGGATCCGGATCCTT-3′; strand II: 5′-TTTAGTGAGGGTTAATCATACGATTTAGGTGAAAGGATCCGGATCCTT-3′; strand III: 5′-TCACCTAAATCGTATGGGAGCTCTGCTTATATAAGGATCCGGATCCTT-3′; strand IV: 5′-ATATAAGCAGAGCTCCTAGAAGGCACAGTCGAAAGGATCCGGATCCTT-3′; strand V: 5′-TCGACTGTGCCTTCTATAATACGACTCACTATAAGGATCCGGATCCTT-3′; strand V′: 5′-TCGACTGTGCCTTCTAGTTATTGTGCTGTCTCAAGGATCCGGATCCTT-3′; strand VI: 5′-GAGACAGCACAATAACTAATACGACTCACTATGGCTATAGCACATGGGTAAAACGAC-3′; FITC-strand I: 5′-FITC-ATAGTGAGTCGTATTAATTAACCCTCACTAAAAAGGATCCGGATCCTT-3′; MUC1 aptamer: 5′-GGCTATAGCACATGGGTAAAACGAC-3′. All oligonucleotides were purchased from MDBio, Taiwan.

Formation of Icosahedral DNA Complexes. To assemble the DNA-icosa and Apt-DNA-icosa, groups of five and six DNA strands each, respectively, were mixed with equal molecular concentration (1000 nM for each strand) in a tris-acetic-EDTA-Mg^{2+} (TAE/Mg^{2+}) buffer that contained 40 mM Tris base (pH 8.0), 20 mM acetic acid, 2 mM EDTA, and 12.5 mM magnesium chloride. The DNA samples were heated to 94 °C and then cooled to room temperature (24 °C). Although it took just 2.5 h for the samples to cool from 94 to 24 °C, 48 h were allotted to the cooling period. FITC-Apt-DNA-icosa was prepared using the same six DNA strands as those for Apt-DNA-icosa, except strand I was replaced by FITC-strand I. The assembled DNA samples were directly used for characterization, without further fractionation or purification.

Characterization of DNA Icosahedra. For DLS, 12 μL of each DNA sample was measured by a particle size analyzer (90 Plus, Brookhaven Instruments Corp.).

Agarose (2%) gel electrophoreses were run at room temperature. The gel was stained with ethidium bromide after electrophoresis, and the images were taken with an Alpha Imager. From the gel image, assembling yields were obtained with AlphaEaseFC image-processing software.

For TEM, 12 μL of each DNA sample was loaded onto the grid (Electron Microscopy Sciences), and extra TAE/Mg^{2+} buffer was absorbed by a nitrocellulose membrane. The loaded grid was stored in a drybox at room temperature for two weeks with negative staining (5% (w/v) ammonium molybdate, 0.1% (w/v) trehalose). The samples were observed with TEM (Hitachi H-7650) at an accelerating voltage of 80 kV.

Doxorubicin Intercalation. For doxorubicin intercalation into DNA-icosa and Apt-DNA-icosa, doxorubicin (1 to 1000 μM) was mixed with DNA-icosa (32 μM) and Apt-DNA-icosa (32 μM) for 1 h and then centrifuged at 16000*g* at room temperature for 10 min. The pellets were then lysed with DMSO for analysis. The amounts of doxorubicin in Doxo@DNA-icosa and Doxo@Apt-DNA-icosa were determined by measuring the emission (570 nm) of doxorubicin using a microplate reader (Infinite M 200, TECAN).

Cells. For cell culture and cell treatment, regular growth medium consisting of Nutrition Mixture F12 Ham (Sigma) was used for CHO-K1 cells, and low-glucose DMEM (GIBCO) was used for MCF-7. Both media were supplemented with 10% fetal bovine serum (FBS) (GIBCO), 100 U/mL penicillin, and 100 μg/mL streptomycin. All cultures were kept in an atmosphere of 5% CO_2 and 95% air at 37 °C. For co-culture of CHO-K1 and MCF-7 cells, Nutrition Mixture F12 Ham medium was used.

Flow Cytometry Analysis. CHO-K1 cells or MCF-7 cells were seeded at 1×10^5 cells per well in a 12-well plate and then cultured for 24 h. Cells were treated with vehicle (PBS), doxorubicin (Doxo), Doxo@DNA-icosa, or Doxo@Apt-DNA-icosa combined without or with free aptamer in growth media for 30 min and washed with PBS for flow cytometry analysis (FACSCalibur, BD).

Confocal Microscopic Analysis. For selective binding and delivery of Doxo@Apt-DNA-icosa, CHO-K1 cells or MCF-7 cells were seeded at 2×10^5 cells per well onto the glass cover-slide coated with polylysine in a six-well plate and then cultured for 24 h. Cells were treated with doxorubicin (Doxo), Doxo@DNA-icosa, or Doxo@Apt-DNA-icosa in growth media for 30 min, and the nuclei of cells were labeled with DAPI (Invitrogen).

For co-culture of CHO-K1 and MCF-7 cells, CHO-K1 cells but not MCF-7 cells were prelabeled with green dye (VybrantTM DiO cell-labeling solution, Invitrogen). Both cells (2×10^5 cells for each cell line per well) were then seeded onto the glass cover-slide coated with polylysine in a six-well plate and then cultured for 24 h. Cells were treated with vehicle (PBS as control), doxorubicin, Doxo@DNA-icosa, and Doxo@Apt-DNA-icosa in growth media for 30 min.

For studying internal localization of FITC-Apt-DNA-icosa, MCF-7 cells (2×10^5 cells) were seeded onto the glass cover-slide coated with polylysine in a six-well plate and then cultured for 24 h. MCF-7 cells were treated with FITC-Apt-DNA-icosa in growth media for 30 min and then labeled with LysoTracker Red (Molecular Probes).

After the above treatments and labeling, cells were washed with PBS and then processed for confocal imaging (FluoView FV10i, Olympus).

Cell Viability Assay. For the cell viability assay, cytotoxicity was assessed using the 3-[4,5-dimethylthiazol-2-yl]-2,5-diphenyltetrazolium bromide (MTT) reduction assay; 1×10^4 cells were seeded in a 96-well plate and then cultured for 24 h. After incubation with doxorubicin, Doxo@DNA-icosa, and Doxo@Apt-DNA-icosa in growth media for 30 min, cells were washed with PBS and cultured in growth medium for 48 h. Cells were then incubated with fresh serum-free medium containing 0.5 mg/mL MTT for 1 h at 37 °C for the cytotoxicity assay. The absorbance at 570 nm was measured using a microplate reader.

Acknowledgment. This study was supported by a grant from the National Health Research Institutes (NM-098-PP-09, NM-099-PP-09, and NM-099-PP-12), Taiwan. M.C. worked under the graduate program in Biotechnology in Medicine sponsored by National Tsing-Hua University and the National Health Research Institutes.

Supporting Information Available: Possible mechanism for the controlled release of doxorubicin from DNA-icosa-intercalated and Apt-DNA-icosa-intercalated molecules, the proposed assembly process of Apt-DNA-icosa, stability, characterization, and yield of DNA assemblies, and statistical analysis of the size of the observed particles visualized by TEM. This material is available free of charge *via* the Internet at http://pubs.acs.org.

REFERENCES AND NOTES

1. Winfree, E.; Liu, F. R.; Wenzler, L. A.; Seeman, N. C. Design and Self-Assembly of Two-Dimensional DNA Crystals. *Nature* **1998**, *394*, 539–544.
2. Yan, H.; Park, S. H.; Finkelstein, G.; Reif, J. H.; LeBean, T. H. DNA-Templated Self-Assembly of Protein Arrays and Highly Conductive Nanowires. *Science* **2003**, *301*, 1882–1884.
3. Rothemund, P. W. K.; Papadakis, N.; Winfree, E. Algorithmic Self-Assembly of DNA Sierpinski Triangles. *PLoS Biol.* **2004**, *2*, e424.
4. Rothemund, P. W. K. Folding DNA to Create Nanoscale Shapes and Patterns. *Nature* **2006**, *440*, 297–302.

5. Chen, J. H.; Seeman, N. C. Synthesis from DNA of a Molecule with the Connectivity of a Cube. *Nature* **1991**, *350*, 631–633.
6. Zhang, Y. W.; Seeman, N. C. Construction of a DNA-Truncated Octahedron. *J. Am. Chem. Soc.* **1994**, *116*, 1661–1669.
7. Shih, W. M.; Quispe, J. D.; Joyce, G. F. A 1.7-Kilobase Single-Stranded DNA that Folds into a Nanoscale Octahedron. *Nature* **2004**, *427*, 618–621.
8. Goodman, R. P.; Berry, R. M.; Turberfield, A. J. The Single-Step Synthesis of a DNA Tetrahedron. *Chem. Commun.* **2004**, 1372–1373.
9. Goodman, R. P.; Schaap, I. A. T.; Tardin, C. F.; Erben, C. M.; Berry, R. M.; Schmidt, C. F.; Turberfield, A. J. Rapid Chiral Assembly of Rigid DNA Building Blocks for Molecular Nanofabrication. *Science* **2005**, *310*, 1661–1665.
10. Liedl, T.; Högberg, B.; Tytell, J.; Ingber, D. E.; Shih, W. M. Self-Assembly of Three-Dimensional Prestressed Tensegrity Structures from DNA. *Nat. Nanotechnol.* **2010**, *5*, 520–524.
11. Bhatia, D.; Mehtab, S.; Krishnan, R.; Indi, S. S.; Basu, A.; Krishnan, Y. Icosahedral DNA Nanocapsules by Modual Assembly. *Angew. Chem., Int. Ed.* **2009**, *48*, 4134–4137.
12. Guo, P. The Emerging Field of RNA Nanotechnology. *Nat. Nanotechnol.* **2010**, *5*, 833–842.
13. Afonin, K. A.; Bindewald, E.; Yaghoubian, A. J.; Voss, N.; Jacovetty, E.; Shapiro, B. A.; Jaeger, L. *In Vitro* Assembly of Cubic RNA-Based Scaffolds Designed in Silico. *Nat. Nanotechnol.* **2010**, *5*, 676–682.
14. Grabow, W. W.; Zakrevsky, P.; Afonin, K. A.; Chworos, A; Shapiro, B. A.; Jaeger, L. Self-Assembling RNA Nanorings Based on RNAI/II Inverse Kissing Complexes. *Nano Lett.* **2011**, *11*, 878–887.
15. Zhang, C.; Su, M.; He, Y.; Zhao, X.; Fang, P. A.; Ribbe, A. E.; Jiang, W.; Mao, C. D. Conformational Flexibility Facilitates Self-Assembly of Complex DNA Nanostructures. *Proc. Natl. Acad. Sci. U. S. A.* **2008**, *105*, 10665–10669.
16. Ingber, D. E. Tensegrity: The Architectural Basis of Cellular Mechanotransduction. *Annu. Rev. Physiol.* **1997**, *59*, 575–599.
17. Liu, D.; Wang, M. S.; Deng, Z. X.; Walulu, R.; Mao, C. D. Tensegrity: Construction of Rigid DNA Triangles with Flexible Four-Arm DNA Junctions. *J. Am. Chem. Soc.* **1998**, *126*, 2324–2325.
18. Feigon, J.; Dieckmann, T.; Smith, F. W. Aptamer Structures from A to Zeta. *Chem. Biol.* **1996**, *3*, 611–617.
19. Breaker, R. R. DNA Aptamers and DNA Enzymes. *Curr. Opin. Chem. Biol.* **1997**, *1*, 26–31.
20. Bartlett, N. L; Petroni, G. R.; Parker, B. A.; Wagner, N. D.; Gockerman, J. P; Omura, G. A.; Canellos, G. P.; Robert, M.; Johnson, J. L.; Peterson, B. A. Dose-Escalated Cyclophosphamide, Doxorubcin, Vincristine, Prednisone, and Etoposide (CHOPE) Chemotherapy for Patients with Lymphoma: Cancer and Leukemia Group B Studies 8852 and 8854. *Cancer* **2001**, *92*, 207–217.
21. Edmonson, J. H.; Petersen, I. A.; Shives, T. C.; Mahoney, M. R.; Rock, M. G.; Haddock, M. G.; Sim, F. H.; Maples, W. J.; O'Connor, M. I.; Gunderson, L. L.; *et al*. Chemotherapy, Irradiation, and Sugery for Function-Preserving Therapy of Primary Extremity Soft Tissue Sarcomas: Initial Treatment with Ifosfamide, Mitomycin, Doxorubcin, and Cisplatin Plus Granulocyte Macrophage-Colony-Stimulating Factor. *Cancer* **2002**, *94*, 786–792.
22. Mishima, Y.; Nagasaki, E.; Terui, Y.; Irie, T.; Takahashi, S.; Ito, Y.; Oguchi, M.; Kawabata, K.; Kamata, S.; Hatake, K. Combination Chemotherapy (Cyclophosphamide, Doxorubcin, and Vincristine with Continuous-Infusion Cisplatin and Etoposide) and Radiotherapy with Stem Cell Support Can Be Benificial for Adolescents and Adults with Estheisoneuroblastoma. *Cancer* **2004**, *101*, 1437–1444.
23. Huybrechts, M.; Symann, M.; Trouet, A. Effects of Daunorubicin and Doxorubicin, Free and Associated with DNA, on Lemopoietic Stem Cells. *Cancer Res.* **1979**, *39*, 3738–3743.
24. Bodley, A.; Liu, L. F.; Tsrael, M.; Seshadri, R.; Koseki, Y.; Giuliani, F. C.; Kirschenbaum, S.; Silber, R.; Potmesil, M. DNA Topoisomerase II-Mediated Interaction of Doxorubicin and Daunorubicin Congeners with DNA. *Cancer Res.* **1989**, *49*, 5969–5978.
25. Brayman, M.; Thathiah, A.; Carson, D. D. MUC1: a Multifunctional Cell Surface Component of Reproductive Tissue Epithelia. *Reprod. Biol. Endocrinol.* **2004**, *2*, 4.
26. Gendler, S. J. MUC1, the Renaissance Molecule. *J. Mammary Gland Biol. Neoplasia* **2001**, *6*, 339–353.
27. Litvinov, S. V.; Hilkens, J. The Epithelial Sialomucin, Episialin, Is Sialylated during Recycling. *J. Biol. Chem.* **1993**, *268*, 21364–21371.
28. Altschuler, Y.; Kinlough, C. L.; Poland, P. A.; Bruns, J. B.; Apodaca, G.; Weisz, O. A.; Hughey, R. P. Clathrin-Mediated Endocytosis of MUC1 Is Modulated by Its Glycosylation State. *Mol. Biol. Cell* **2000**, *11*, 819–831.
29. Ferreira, C. S.; Cheung, M. C.; Missailidis, S.; Bisland, S.; Gariépy, J. Phototoxic Aptamers Selectively Enter and Kill Epithelial Cancer Cells. *Nucleic Acids Res.* **2009**, *37*, 866–876.